INTERNATIONAL JOURNAL OF HYDROGEN ENERGY 39 (2014) 7326–7337

Available online at www.sciencedirect.com

ScienceDirect

journal homepage: www.elsevier.com/locate/he

Formic acid oxidation reaction on a Pd_xNi_y bimetallic nanoparticle catalyst prepared by a thermal decomposition process using ionic liquids as the solvent

Keqiang Ding [a,*], *Lu Liu* [a], *Yanli Cao* [a], *Xingru Yan* [b], *Huige Wei* [b], *Zhanhu Guo* [b,**]

[a] *College of Chemistry and Materials Science, Hebei Normal University, Shijiazhuang 050024, PR China*
[b] *Integrated Composites Laboratory (ICL), Dan F. Smith Department of Chemical Engineering, Lamar University, Beaumont, TX 77710, USA*

ARTICLE INFO

Article history:
Received 28 January 2014
Received in revised form
28 February 2014
Accepted 8 March 2014
Available online 2 April 2014

Keywords:
Thermal decomposition
Pd_xNi_y bimetallic nanoparticles
Formic acid oxidation reaction
Electrocatalysis

ABSTRACT

The nano-catalysts of Pd_xNi_y bimetallic nanoparticles (NPs, the nominal atomic ratios of Pd to Ni are 2:1, 3:2 and 1:1) supported on multi-walled carbon nanotubes (MWCNTs) (denoted as Pd_xNi_y/MWCNTs) have been synthesized by a thermal decomposition process using room temperature ionic liquids (RTILs) of N-butylpyridinium tetrafluoroborate ($BPyBF_4$) as the solvent. X-ray diffraction (XRD), scanning electron microscope (SEM) and transmission electron microscopy (TEM) were employed to characterize the morphology of the samples, revealing that the prepared Pd_xNi_y NPs were quite uniformly dispersed on the surface of MWCNTs with an average particle size of ~8.0 nm. Formic acid oxidation reaction (FAOR) was investigated on the as-prepared catalysts by using cyclic voltammetry (CV) and electrochemical impedance spectroscopy (EIS), demonstrating that the peak current on the Pd_3Ni_2/MWCNTs catalyst was about three times higher than that on the Pd/MWCNTs. The lower electrode potential and easier hydrogen evolution, based on the results obtained from chronopotentiometry and CV, respectively, were thought as the main reasons for the excellent electrocatalysis of the Pd_3Ni_2/MWCNTs toward formic acid oxidation reaction (FAOR) when compared to other samples.

Introduction

Although numerous kinds of platinum (Pt) or palladium (Pd) based bi- or tri-metallic nanoparticles (NPs) have been used as catalysts for small organic molecule oxidation reactions, the exact role of the second or third metal in the obtained composite (or alloyed) NPs toward small organic molecule oxidation reaction still remains unclear [1]. Compared to the direct liquid (mainly including methanol and ethanol) fuel cells,

* *Corresponding author*. Tel.: +86 311 80787400.
** *Corresponding author*. Tel.: +1 409 880 7654.
E-mail addresses: dkeqiang@263.net (K. Ding), zhanhu.guo@lamar.edu (Z. Guo).

http://dx.doi.org/10.1016/j.ijhydene.2014.03.026

formic acid-based fuel cells have been paid much attention essentially due to its unique advantages such as nontoxicity, inflammability at room temperature, higher theoretical open circuit potential, lower crossover through the membrane and the easy fuel storage and transport [2]. Thus, developing novel catalysts for formic acid oxidation reaction (FAOR) has become attractive in the research field of electrochemistry [3]. Although platinum (Pt) has been widely employed as catalysts for small organic molecule oxidation reactions, the high cost and limited supply of Pt have limited its application in fuel cells [4].

Palladium (Pd) at nanoscale size has demonstrated its unique ability to catalyze the oxidation of formic acid in fuel cells in 1987 [5]. Recently, many methods to synthesize Pd NPs have been reported. For example, Wang et al. [6] reported a facile method to synthesize Pd NPs supported on graphene ribbon (GR), in which Na_2PdCl_4 was employed as the precursor and graphene ribbon itself served as the reducing reagent, stabilizer, and catalyst support for Pd. And the as-synthesized Pd/GR electrocatalysts showed increased electrochemical surface area and significantly enhanced catalytic activity for FAOR compared with the conventional Pd/C electrocatalysts in terms of peak current density and peak potential. Hong et al. [7] reported that the carbon supported Pd NPs could be produced via an ultrasound assisted way at room temperature, where chloropalladic acid and ethylene glycol were utilized as the precursor and reducing reagent, respectively. However, recent works revealed that the electrocatalytic stability of the Pd catalyst used in direct formic acid fuel cells (DFAFCs) still remains unsatisfactory. Thus, to augment the electrocatalytic stability of the Pd catalyst, various Pd-based catalysts, such as Pd–Ir [8], Pd–Au [9] and Pd–Co [10] have been developed, and the second or third metal can remarkably improve the electrocatalytic performance of the Pd catalyst. Among the Pd-based bimetallic catalysts, Pd–Ni catalysts have been prepared by various methods. The first is the chemical reduction reaction. For example, Scott et al. [11] reported the carbon nanofibers (CNFs) supported Pd–Ni nanoparticles that were prepared by a chemical reduction reaction using $NaBH_4$ as the reducing agent, in which the electrocatalytic activity of the Pd–Ni/CNF for the oxidation of ethanol instead of formic acid was examined by cyclic voltammetry. Recently, Shen et al. [12] addressed the synthesis of a carbon supported Pd–Ni catalyst via a high-temperature calcination and chemical etching method. The electrocatalysis of the Pd–Ni/C catalyst for formic acid oxidation was much better than that of the Pd/C catalyst. The second method is the electrochemical reduction reaction. For instance, Xiao et al. [13] reported the fabrication of Pd–Ni alloy nanowires using an electrochemical step edge decoration method, in which the plating solution contained $Pd(NH_3)_4Cl_2$ and $NiSO_4 \cdot 6H_2O$.

Due to their excellent features including low-volatility, non-toxicity and higher conductivity compared to common organic solvents, and higher solubility for organic substances compared with aqueous solutions, room temperature ionic liquids (RTILs) have attracted much attention recently [14]. For example, RTILs have been used as solvent in organic synthesis [15] and electrolyte [16] in electrochemistry. To our knowledge, except our previous work [17], reports on the application of RTILs in a thermal decomposition process are rare.

Compared with CNFs [18] and graphene [19], carbon nanotubes (CNTs) have attracted a great deal of attention [20] due to their unique properties, such as high specific surface area, electrical conductivity, and good thermal and chemical stability, which make them a good catalyst support for fuel cells [21]. For example, immobilizing metal NPs on CNTs has become an interesting research field mainly due to the key roles of CNTs and metal NPs in the field of electrocatalysis, biosensors and so on [22]. To the best of our knowledge, the immobilization of Pd_xNi_y composite NPs on CNTs by a method of thermal decomposition has not been reported; though we have anchored platinum (Pt) NPs on the surface of MWCNTs by a thermal decomposition process using distilled water as solvent successfully [23].

Although the Pd-based catalysts were reported to possess much better electrocatalytic activity for formic acid oxidation than that of the Pt-based catalysts [3], the exact catalysis mechanism of the Pd-based binary or ternary metal catalysts toward FAOR is still unclear. For example, Li et al. [24] reported that the enhanced catalysis exhibited by the Pd–Ni alloy should be ascribed to the largely increased electrochemical active surface area (EASA) from smaller particle size and better dispersion combining with the electronic modification effect of nickel. Shen et al. [12] reckoned that the Pd–Ni/C catalyst could be significantly protected from CO poisoning, which can lead to excellent electrocatalytic stability. The inconsistent interpretation on the electrocatalysis of Pd–Ni towards FAOR is also the main reason that stimulates us to further investigate the catalyst of Pd–Ni.

In this paper, three kinds of Pd_xNi_y/MWCNT nanocomposite catalysts with various atomic ratios of Pd to Ni were prepared by a simple thermal decomposition method, in which RTILs of N-butylpyridinium tetrafluoroborate ($BPyBF_4$) was used as the solvent. The morphology and crystalline structures of the as-synthesized Pd_xNi_y/MWCNT nanocomposites were probed by scanning electron microscopy (SEM), transmission electron microscopy (TEM) and x-ray diffraction (XRD). The electrochemical activities of the as-prepared catalysts for FAOR were investigated by cyclic voltammetry (CV), chronoamperometry and electrochemical impedance spectroscope (EIS). The possible reasons for the excellent electrocatalytic activity of the Pd_3Ni_2/MWCNTs towards FAOR were also discussed.

Experiment

Materials

MWCNTs (purity >95%) with an average diameter of 10–20 nm were purchased from Shenzhen nanotech port Co., Ltd. (China). Room temperature ionic liquid of N-butylpyridinium tetrafluoroborate ($BPyBF_4$) with a purity of more than 99% was obtained from Hangzhou Chemer Chemical Co., Ltd. (China). All the electrodes were purchased from Tianjin Aida Co., Ltd (China). All the chemicals were of analytical grade and used as-received without any further treatment. Deionized water was used to prepare the aqueous solutions.

Preparation of Pd_xNi_y bimetallic nanocomposite particles

Firstly, 6 mg $PdCl_2$ was dissolved in 4 mL $BPyBF_4$ to prepare the RTILs solution, and then a proper amount of $Ni(CH_3COO)_2{\cdot}4H_2O$ was dissolved in the above solution. It should be mentioned that the amount of $Ni(CH_3COO)_2{\cdot}4H_2O$ employed was determined on the atomic ratios of Pd to Ni (i.e., atomic ratios of Pd to Ni were fixed at 2:1, 3:2 and 1:1, respectively). Subsequently, 10 mg MWCNTs were added to the above solution, generating a suspension solution, following 30 min ultrasonication. The resultant suspension solution was placed in a home-made autoclave at room temperature, and then the well-sealed autoclave was transferred to a muffle furnace. The muffle furnace was maintained for 3 h to complete the thermal decomposition process at 200 °C, which was carried out in an SRJX-8-13 muffle furnace equipped with a KSY 12-16 furnace temperature controller. After cooling down to room temperature, the filtered samples were thoroughly washed copiously with distilled water and dried in ambient condition to generate MWCNTs supported Pd_xNi_y catalysts (denoted as Pd_xNi_y/MWCNTs). The Pd/MWCNTs and Ni/MWCNTs were also prepared following the same procedures for comparison.

Fabrication of Pd_xNi_y/MWCNTs modified electrode

A glassy carbon (GC) electrode with a cross-sectional area of 0.07 cm^2 was polished to a mirror finish with 50 nm alumina nanopowder suspensions, and then served as a substrate for the working electrode. The working electrodes were fabricated by coating catalyst ink onto a GC electrode. The catalysts ink was prepared by dispersing 1 mg catalyst in 1 mL Nafion ethanol solution (0.1 wt%). And after ultrasonication for 20 min, about 15 μL ink was added on the surface of the GC electrode. Finally, the Pd_xNi_y/MWCNTs-coated GC electrode was fabricated after drying in air atmosphere.

Characterizations

The particle morphology was observed by scanning electron microscopy (SEM, HITACHI, S-570) and transmission electron microscopy (TEM, HITACHI, H-7650). XRD analysis of the catalysts was carried out on a Bruker D8 ADVANCE X-ray diffractometer equipped with a Cu Kα source ($\lambda = 0.154$ nm) at 40 kV and 30 mA. The 2θ angular region between 10 and 90° was explored at a scan rate of 1°/step. Fourier transform infrared spectrometry (FT-IR) measurements were carried out on a Hitachi FT-IR-8900 spectrometer (Japan). Energy Dispersive X-Ray Spectroscopy (EDX) spectrum analysis were carried out on an X-ray energy instrument (EDAX, PV-9900, USA).

Electrochemical measurements, including cyclic voltammetry (CV), chronoamperometry, chronopotentiometry and electrochemical impedance spectroscopy (EIS) were carried out on a CHI 660B electrochemical working station (Shanghai Chenhua Apparatus, China) connected to a personal computer. EIS was performed in the frequency range from 0.1 to 10^5 Hz with an amplitude of 5 mV at the open circuit potential.

A conventional three-electrode system was employed, in which a Pd_xNi_y/MWCNTs modified GC electrode and a platinum wire were used as the working electrode and counter electrode, respectively. It should be noted that the reference electrode was an Hg/Hg_2SO_4 saturated-K_2SO_4 electrode (0.64 V *vs.* NHE). All potentials in this paper were reported with respect to this reference electrode. A solution of 0.5 M H_2SO_4 containing 0.5 M HCOOH was used to study formic acid oxidation activity. Prior to each electrochemical test, the electrolyte was bubbled with high purity nitrogen for 30 min to avoid the influence of oxygen dissolved in the electrolyte. All the experiments were carried out at room temperature.

Results and discussion

XRD analysis

The XRD patterns of the as-prepared samples are illustrated in Fig. 1. For pure MWCNTs, the diffraction peak at around 26° can only be assigned to the (002) facet of MWCNTs [7,25]. For the Pd/MWCNTs, four typical peaks corresponding to the planes (111), (200), (220) and (311) are observed at 2θ values of about 39.9, 47, 68 and 82°, respectively, which are the characteristics of the face centered cubic (fcc) crystalline Pd (JCPDS, Card No. 01-089-4897). This result is well consistent with the previous report [7]. Interestingly, for the other three catalysts of Pd_xNi_y/MWCNTs, only the characteristic diffraction peaks of fcc Pd are displayed compared with that of Pd/MWCNTs, suggesting that the addition of Ni did not change the crystalline structure of Pd though the intensities of all the patterns are varied when altering the atomic ratios of Pd to Ni. However, no diffraction peaks of metallic Ni or its oxides/hydroxides are observed, suggesting that the amount of Ni-contained substance is too small to be detected, or their existence in amorphous phases [26]. Also, due to the properties of RTILs of N-butylpyridinium tetrafluoroborate ($BPyBF_4$), oxygen and water in the above preparation system are very limited compared to the aqueous system, which probably should be responsible for the absence of Ni oxides/hydroxides in the resultant samples. Evidently, compared to pure MWCNTs, the intensity of the diffraction peak (002) facet is greatly attenuated after the process, as shown in the circled

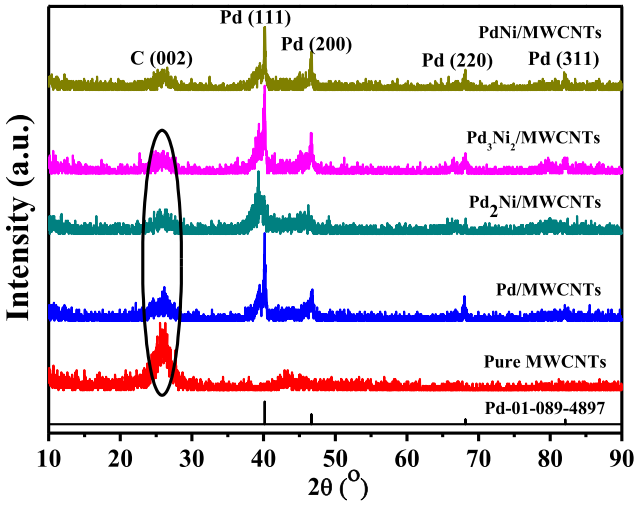

Fig. 1 – XRD patterns of pure MWCNTs, Pd/MWCNTs, Pd_2Ni/MWCNTs, Pd_3Ni_2/MWCNTs and PdNi/MWCNTs.

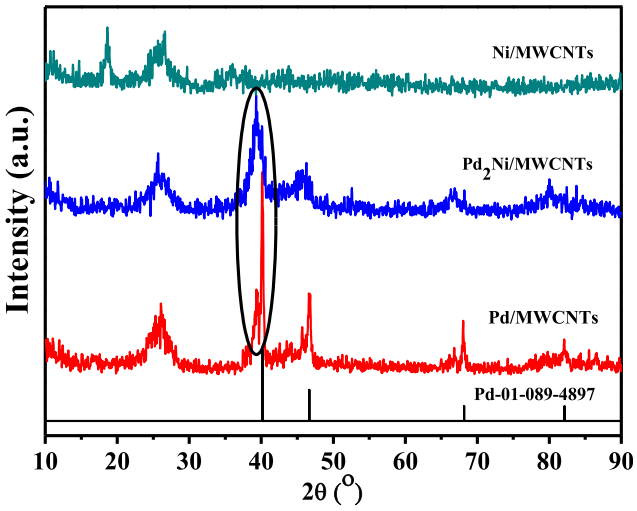

Fig. 2 – XRD patterns of Ni/MWCNTs, Pd_2Ni/MWCNTs, Pd/MWCNTs and the standard pattern of Pd.

part, implying that the structure of MWCNTs was changed during the thermal decomposition. Meanwhile, a close check reveals that the intensity of all the diffraction peaks for the Pd_3Ni_2/MWCNTs, such as the peak at around 39.9°, is obviously higher than that of PdNi/MWCNTs and Pd_2Ni/MWCNTs, indicating that the crystallinity of Pd_3Ni_2/MWCNTs is the best among all the three catalysts [27].

For comparison, the magnified XRD patterns of the Ni/MWCNTs, Pd/MWCNTs and Pd_2Ni/MWCNTs are displayed in Fig. 2. For Ni/MWCNTs, no diffraction peaks of metallic Ni are observed due to the too small amount of the well defined crystalline metallic Ni. Significantly, an obvious diffraction peak shift is observed to a lower instead of higher scanning angle in the XRD patter for the Pd_2Ni/MWCNTs than that of Pd/MWCNTs. The decrease in 2θ value should result in an increase in the lattice parameters based on the Bragg's law and the observed shift of the diffraction peak toward lower angle is probably due to the substitution of one Pd by Ni [28].

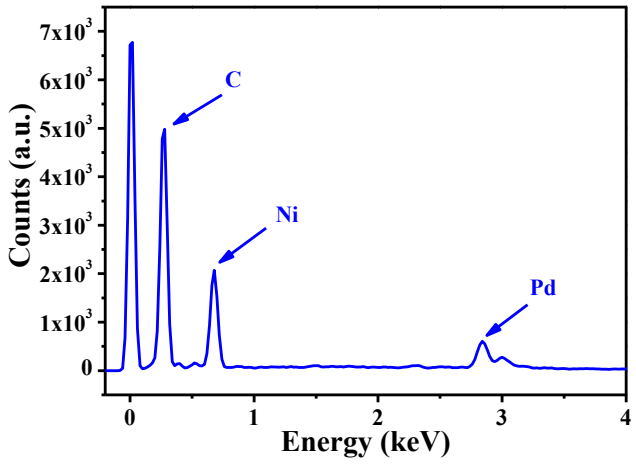

Fig. 3 – EDX spectra for the as-prepared Pd_3Ni_2/MWCNTs catalyst.

According to the Scherrer formula using Equation (1) [29], the average crystallite size of the catalysts was also estimated from Pd (111) peak:

$$d\left(\text{Å}\right) = \frac{\kappa\lambda}{\beta\cos\theta} \quad (1)$$

where κ is a coefficient (0.9), λ the wavelength of X-ray used (1.54056 Å), β the full-width half maximum (FWHM) and θ is the angle at the position of peak maximum. The calculated particle size, based on (111) plane for Pd/MWCNTs, Pd_2Ni/MWCNTs, Pd_3Ni_2/MWCNTs and PdNi/MWCNTs, is 17.0, 8.20, 7.60 and 10.0 nm, respectively. Thus, the particle size of Pd_3Ni_2/MWCNTs is the smallest among all the prepared samples, indicating a larger surface area relative to other catalysts at the same particle loadings.

The typical EDX spectrum for the catalyst of Pd_3Ni_2/MWCNTs is presented in Fig. 3, which confirms the presence of element C, Pd and Ni in the as-prepared catalyst. According to the results of EDX measurement, Pd_3Ni_2/MWCNTs catalyst

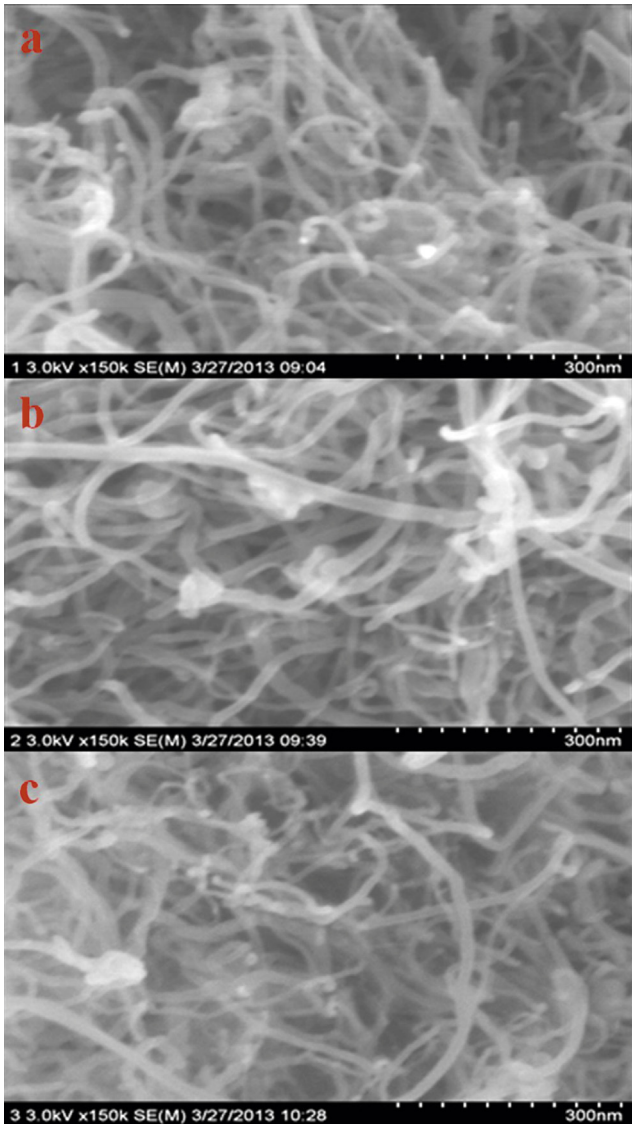

Fig. 4 – SEM images of (a) Pd_2Ni/MWCNTs, (b) Pd_3Ni_2/MWCNTs, (c) PdNi/MWCNTs.

prepared in this work contains 25.5% (atomic content) of Pd and 9.5% of Ni, which is larger than the stoichiometric ratio of 3:2 used in the starting materials. Therefore, the atomic ratio of Pd to Ni in the prepared Pd_xNi_y/MWCNTs should be the nominal ratio rather than the real ratio in the resultant samples.

Morphology characterization

Fig. 4 shows the SEM morphologies of the three catalysts. Compared to pure MWCNTs, some white dots are observed on the surface of MWCNTs after the process, indicating the formation of nanoparticles on the surface of MWCNTs during the thermal decomposition process. This result is consistent with our previous report [23]. The TEM microstructures of these three typical samples are illustrated in Fig. 5. The as-prepared nanoparticles are observed to be uniformly dispersed on the outer walls of the MWCNTs, and no obvious agglomerations are found. Compared to water, $BPyBF_4$ has a lower dielectric constant [30]. Generally, the low charges and asymmetrically distributed charges were deemed as the key factors to produce nanoparticle aggregation [31], which is similar to the case described by Wang et al. [32]. The solvent of $BPyBF_4$ can decrease the surface charge of the Pd_xNi_y nanoparticles, thus the newly formed Pd or Ni atoms can migrate from the $BPyBF_4$ to the $BPyBF_4/Pd_xNi_y$ interface in sequence, which can be analogous to the nanoparticle self-assembly at the toluene/water or hexane/water interface in ethanol-mediated methanol [33]. Consequently, the agglomeration of Pd_xNi_y particles is greatly inhibited, generating a uniform dispersion. The particle sizes of the Pd_2Ni/MWCNTs, Pd_3Ni_2/MWCNTs and PdNi/MWCNTs are estimated to be 10.2, 9.2 and 11.0 nm based on the TEM images, respectively. All these estimated particle sizes are slightly larger than those calculated from the XRD patterns, indicating that some nanoparticles were formed by some small crystals.

Electrochemical characterization

Fig. 6 shows the cyclic voltammograms (CVs) of the Pd_xNi_y/MWCNTs catalysts in a solution of 0.5 M H_2SO_4 and 0.5 M HCOOH. No peak is obviously displayed on the pure MWCNTs-coated GC electrode, indicating that formic acid oxidation reaction can not proceed on the MWCNTs. While for other

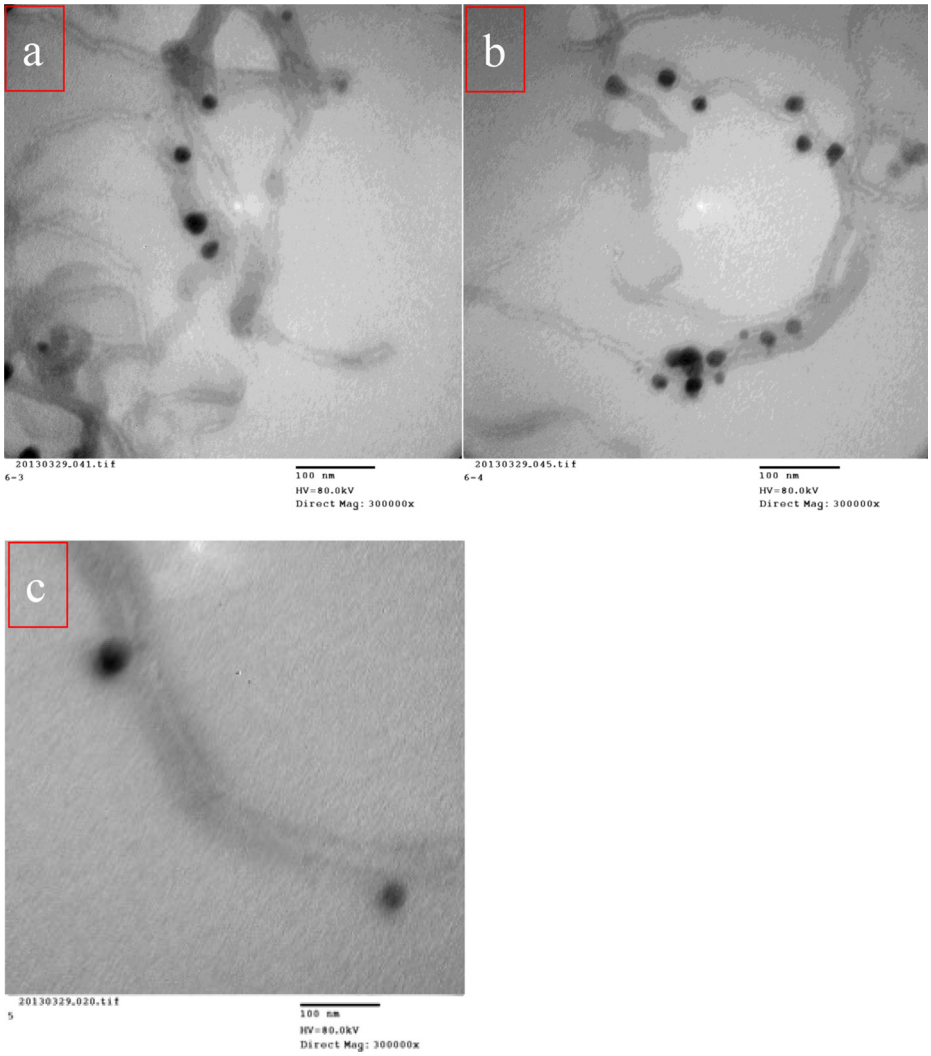

Fig. 5 – TEM microstructures of (a) Pd_2Ni/MWCNTs, (b) Pd_3Ni_2/MWCNTs, (c) PdNi/MWCNTs.

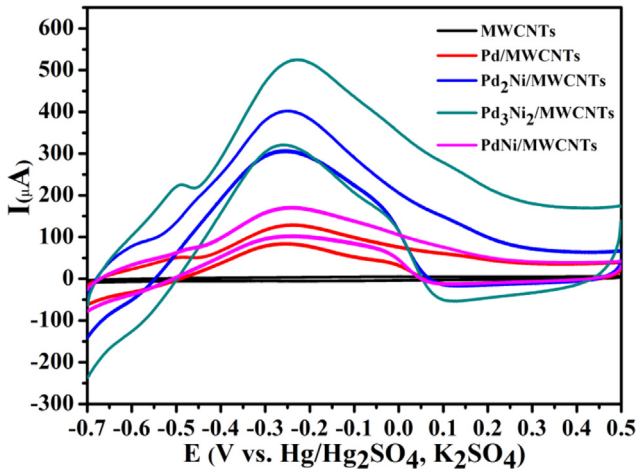

Fig. 6 – CVs obtained on the Pd_xNi_y/MWCNTs coated GC electrode in the solution of 0.5 M H_2SO_4 + 0.5 M HCOOH at the scan rate of 100 mV s^{-1}.

catalysts, peak **1** is centered at ~−0.22 V in the anodic sweep curve, and peak **2** is centered at ~−0.26 V in the cathodic sweep. These two well featured oxidation peaks indicate the FAOR, which is consistent with the previous report [34]. As shown by the green line, for both peak **1** and peak **2**, the largest peak current for the Pd_3Ni_2/MWCNTs catalyst implies the best electro-catalytic ability towards FAOR when compared to other catalysts. Moreover, all the current peaks of FAOR decrease remarkably as plotted by the blue curve when the atomic ratio of Pd to Ni is 2. Fig. 7 displays the CVs of FAOR for the three catalysts, i.e., Pd_3Ni_2/MWCNTs, Pd/MWCNTs and Ni/MWCNTs. It should be mentioned that all the three catalysts were fabricated by the same method, i.e., a thermal decomposition process employing RTILs of $BPyBF_4$ as the solvent. No oxidation peaks are displayed on the catalyst of Ni/MWCNTs-modified GC electrode. Compared to the oxidation peak of FAOR on Pd/MWCNTs, significantly enhanced oxidation peaks are observed on the Pd_3Ni_2/MWCNTs, strongly indicating that a proper amount of Ni added to Pd can promote the electro-catalytic ability of Pd toward FAOR.

Fig. 8 shows the chronoamperometric curves of 0.5 M HCOOH in 0.5 M H_2SO_4 solution at the Pd_xNi_y-coated GC electrodes at −0.25 V with an aim to probe the electrochemical stability of all the as-prepared catalysts toward FAOR [24]. It is observed from Fig. 8 that the currents at the Pd, Pd_2Ni, Pd_3Ni_2 and PdNi/MWCNTs catalyst electrodes are about 0.5, 2.3, 28.7, 16.6 μA at 550 s, respectively. This effectively confirms that the electrocatalytic stability of the Ni-doped Pd/MWCNTs catalysts has a better electrochemical stability than that of pure Pd/MWCNTs, and the Pd_3Ni_2/MWCNTs sample shows the best stability among all the prepared samples when used as a catalyst toward FAOR.

Nyquist plot, one typical curve of electrochemical impedance spectroscopy (EIS) [35], has been widely applied in probing the electrochemical performance of a working electrode. Generally, the semicircle appearing at the high frequency region corresponds to a circuit having a resistance element parallel to a capacitance element. The line with a 45° slope appearing at the lower frequency region corresponds to the Warburg resistance [35]. And the diameter of the semicircle corresponds to the charge transfer resistance (R_{ct}) of the electrochemical reaction occurring at the working electrode. A bigger diameter of the semicircle stands for a larger value of R_{ct}. It can be seen from Fig. 9 that for all the catalysts, the Nyquist plots are constructed by a semicircle at high frequency region and a line close to 90° at the lower frequency region, indicating that all the catalysts of Pd_xNi_y/MWCNTs modified GC electrodes have a similar structure at the interface between the working electrode and electrolyte. A close inspection reveals that the values of the diameter for the catalysts are different from each other. The diameter for the catalysts is about 17.5, 13.2, 11.5 and 13.8 Ω for Pd, Pd_2Ni, Pd_3Ni_2 and PdNi/MWCNTs, respectively. It indicates that Pd_3Ni_2/MWCNTs sample has the best electrocatalysis towards

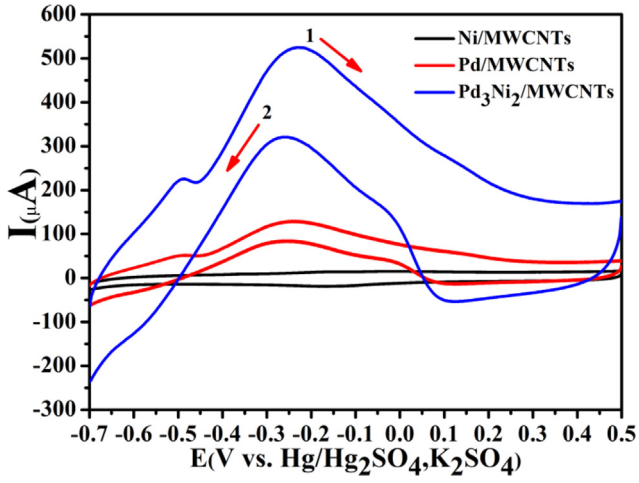

Fig. 7 – CVs obtained on the Ni/MWCNTs, Pd/MWCNTs and Pd_3Ni_2/MWCNTs coated GC electrode in 0.5 M H_2SO_4 + 0.5 M HCOOH at the scan rate of 100 mV s^{-1}.

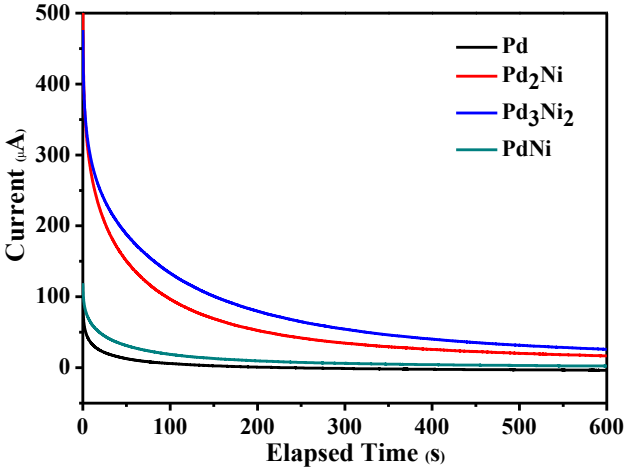

Fig. 8 – Chronoamperometry curves of as-prepared samples-coated GC electrode in 0.5 M H_2SO_4 + 0.5 M HCOOH. (a) Pd/MWCNTs, (b) Pd_2Ni/MWCNTs, (c) Pd_3Ni_2/MWCNTs and (d) PdNi/MWCNTs, respectively.

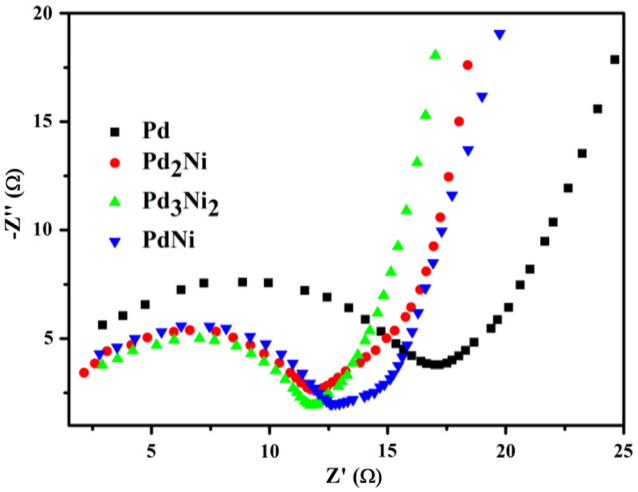

Fig. 9 – Nyquist plots for the catalysts coated GC electrode in 0.5 M H_2SO_4 + 0.5 M HCOOH solution, in which the catalysts are different. (a) Pd/MWCNTs, (b) Pd_2Ni/MWCNTs, (c) Pd_3Ni_2/MWCNTs and (d) PdNi/MWCNTs, respectively.

FAOR, which is consistent with the results obtained from CVs very well, Fig. 6.

To acquire more useful information of the electrical properties of the as-prepared catalysts, Bode plots are presented in Fig. 10. It is evident that all the Pd_xNi_y/MWCNTs coated GC electrodes exhibit one symmetric peaks in the whole frequency region, corresponding to a relaxation process of the electrode/solution interface [36]. The higher phase angles of the Pd_3Ni_2/MWCNTs coated GC electrode (66.5° at 0.02 Hz) compared to other samples (52.0° at 0.02 Hz for Pd/MWCNTs, 58.1° at 0.02 Hz for the PdNi/MWCNTs, 29.0° at 0.02 Hz for the Pd_2Ni/MWCNTs) may be interpreted with respect to the catalyst of Pd_3Ni_2/MWCNTs particles exhibiting more capacitive behavior than that of other samples since ideal capacitive systems should show phase angles of *ca.* −90° [37]. This result proves that the micro-structure of the surface for the Pd_xNi_y/MWCNTs-coated GC electrodes differ from each other.

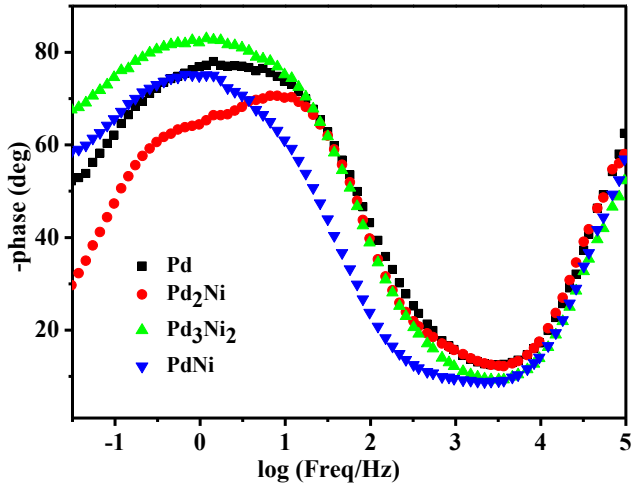

Fig. 10 – Bode plots, obtained for the catalysts coated GC electrode in 0.5 M H_2SO_4 + 0.5 M HCOOH aqueous solution. (a) Pd/MWCNTs, (b) Pd_2Ni/MWCNTs, (c) Pd_3Ni_2/MWCNTs, and (d) PdNi/MWCNTs.

Why did the Pd_xNi_y catalysts with various molar ratios of Pd to Ni show such different electrocatalytic activity toward FAOR? To disclose the possible reasons, CVs of four catalysts in 0.5 M H_2SO_4 are plotted in Fig. 11. Generally, the multiple peaks between −0.7 and −0.4 V are attributed to the hydrogen absorption/desorption (H_{ab}) process and hydrogen adsorption/desorption (H_{ad}) process [38], and the smaller pair of peaks at the more positive potentials was thought to be an indication of real surface area of catalysts. However, in this case, only one pair of peaks appears probably due to the fact that both H_{ab} and H_{ad} have merged into broad H_{ab} peaks [38]. Thus, the area of the peak at around −0.57 V in the negative-direction potential scanning is used to estimate the real active surface of the catalysts approximately. It is clear that the hydrogen absorption peak is not displayed for the pure Pd/MWCNTs, while for the other Ni-doped samples, the area of the H_{ab} peak changes dramatically with the addition of Ni. The largest area of the H_{ab} peak is observed in the catalyst of Pd_3Ni_2/MWCNTs, which are due to the smaller particle size and its better crystallinity as justified by the TEM observations and XRD analysis. For the pure Pd/MWCNTs, a reduction peak appears at around 0 V, corresponding to the reduction of PdO, being consistent with the previous report [3]. Moreover, for the other catalysts of Pd_xNi_y/MWCNTs, no reduction peak of PdO is observed, which is different from the formerly reported data of Pd_xNi_y/C [24]. That is to say, the properties of Pd_xNi_y/MWCNTs prepared by this method using RTILs as the solvent are different from those of previously reported samples. Based on the onset potential (as shown by the red arrow) of the hydrogen absorption peak and its peak area, it can be deduced that the hydrogen absorption process at the Pd_3Ni_2/MWCNTs catalyst proceeded easily compared to those occurring on the other catalysts.

Commonly, the electrooxidation of the formic acid on Pd nanoparticles follows a dual path mechanism, i.e., a dehydrogenation path to the direct formation of CO_2 and a dehydration path, and the adsorption of CO intermediate from the

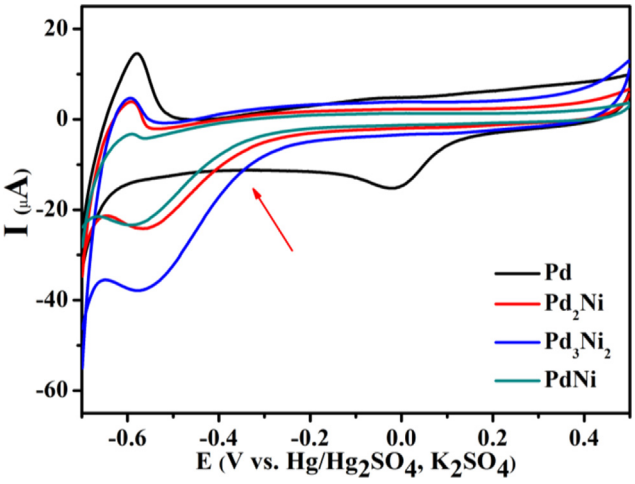

Fig. 11 – CVs of various Pd_xNi_y catalysts modified GC electrodes in 0.5 M H_2SO_4 at a scan rate of 20mV s^{-1}.

dehydration path significantly poisons the activity of Pd catalysts [34] according to the following process:

$$HCOOH \rightarrow CO_2 + 2H^+ + 2e^- \quad (2)$$

$$HCOOH \rightarrow CO_{ads} + H_2O \quad (3)$$

$$CO_{ads} + H_2O \rightarrow CO_2 + 2H^+ + 2e^- \quad (4)$$

While, in our case, at the initial stage of the formic acid oxidation process, for example, at the potential of −0.7 V, more OH^- groups were generated due to the facile process of hydrogen evolution, thus, the protons produced in the process (2) and (4) can be easily consumed by the produced OH^-, leading to an accelerated process of (2) and (4) according to the chemical equilibrium shifting principle of Le Chatelier's principle [39]. In other words, in the vicinity of the surface of Pd_xNi_y nanoparticles, especially for the catalyst of Pd_3Ni_2, a basic micro-environment was fabricated due to the hydrogen evolution process. That is to say, the micro-environment of the surface of Pd_3Ni_2 is different from those of other catalysts, which is responsible for its superior electrocatalysis when compared to other catalysts.

Fig. 12 displays the curves of open circuit potential (OCP) against time. A sharp increment of OCP value is observed within the initial period time of 400 s, and then the value of OCP reaches a stable status. This shape of OCP curves for all the catalysts is analogous to the previously reported one [3]. Evidently, the values of OCP are various when altering the atomic ratios of Pd to Ni. For example, at the working time of 3000 s, the values of COP for the catalysts of Pd, Pd_2Ni, Pd_3Ni_2 and PdNi/MWCNTs are −0.04, −0.098, −0.21 and −0.093 V, respectively. The lowest value of OCP is presented by the sample of Pd_3Ni_2, implying that the electrons can be released from the catalyst of Pd_3Ni_2 easier than the other catalysts according to the Nernst Equation [40]. That is to say, protons can be reduced to generate hydrogen atoms or hydrogen gas facilely on the catalyst of Pd_3Ni_2 relative to other samples, which is testified by the CV curves, Fig. 11.

Fig. 13 displays the chronopotentiometric curves of the various catalysts of Pd_xNi_y coated GC electrodes at a constant current density of 0.14 mA cm^{-2}. Theoretically, the electrode potential will increase to a higher value when charged by a positive current based on the electrochemical principle, as shown in the previous work [41]. For the electrodes modified by Pd, PdNi and Pd_2Ni, the electrode potentials reach as high as 3.28 V at 150 s, and then an almost constant potential is attained at the time of 3500 s. However, for the Pd_3Ni_2 coated electrode, it took almost 1000 s for the electrode to attain a stable electrode potential of 0.42 V, and then the electrode potential increased slowly from 0.42 to 0.95 V within the whole measuring period. The markedly different shape of the V–t curve strongly indicates that these various catalysts exhibited different electrochemical responses when being charged. It is evident that the electrode potential of Pd_3Ni_2 coated electrode remains the lowest value among all the samples. That is to say, even under the charged condition, the catalyst of Pd_3Ni_2 can be thought as a reducing agent, which may facilely reduce the oxidative agents relative to other catalysts. This result probably can account for the enhanced peak current of FAOR observed on the catalyst of Pd_3Ni_2 in some degree. To our knowledge, no reports discussing the electrocatalysis of Pd_xNi_y toward FAOR from the electrochemical viewpoint are published so far. On the other hand, in our previous report [35], it has been proved that the newly generated hydrogen can reduce PdO to Pd, and thus released more active surfaces of Pd towards electrochemical reaction. Similarly, the catalyst of Pd_3Ni_2 was "cleaned" by the newly formed hydrogen atoms (or gas), leading to an increased oxidation peak current of FAOR.

From the viewpoint of electrochemistry, in an acidic medium, a microcell may form where Ni served as the negative electrode and Pd as the positive electrode, respectively. Meanwhile, compared to Pd, Ni is prone to release electrons to form Ni^{2+} since the standard electrode potential of Ni^{2+}/Ni

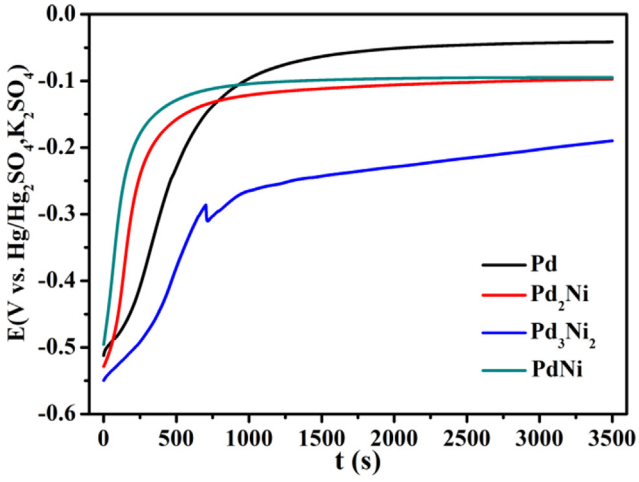

Fig. 12 – Open circuit potentials of various catalyst modified GC electrodes in 0.5 M H_2SO_4 + 0.5 M HCOOH.

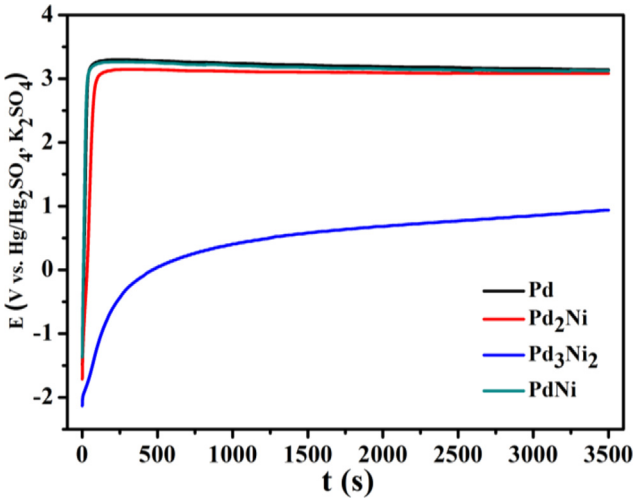

Fig. 13 – Chronopotentiometric curves of FAOR obtained on the as-prepared catalysts in 0.5 M H_2SO_4 + 0.5 M HCOOH at 0.14 mA cm^{-2}.

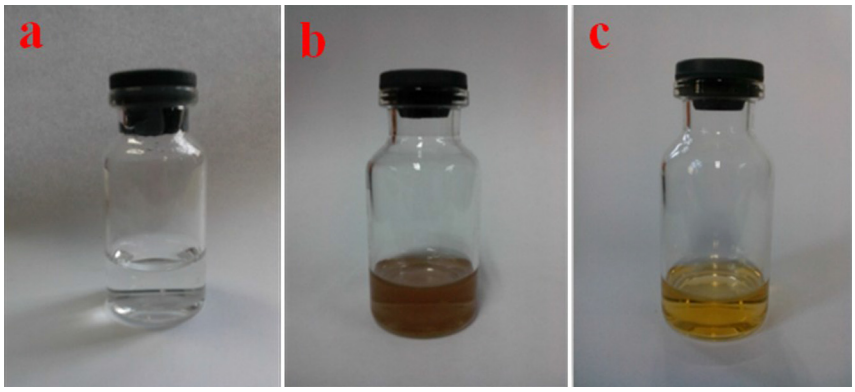

Fig. 14 – Pictures of the samples in experiments (a) pure $BPyBF_4$, (b) $BPyBF_4$ containing Pd^{2+} and Ni^{2+} before thermal decomposition process pyrolysis, and (c) $BPyBF_4$ containing Pd^{2+} and Ni^{2+} after thermal decomposition process.

(−0.257 V *vs.* NHE) is markedly lower than that of Pd/Pd^{2+} (0.915 V *vs.* NHE) [42]. The formed micro-battery may change the micro-environment of the interface between the Pd_3Ni_2/MWCNTs and formic acid when compared to that at the interface between Pd/MWCNTs and formic acid. The newly formed micro-environment may have a significant effect on the FAOR. This new concept of forming a microbattery may provide a novel interpretation for explaining the fact that many binary or ternary composite catalyst particles, such as Pd–Cu [43], Pd–Au [44] and Pd–Co [10], compared to pure metal Pd, have excellent electro-catalysis towards organic small molecules reactions occurring in the fuel cells.

To discuss the mechanism of the thermal decomposition process, photos of the filtered RTILs before and after the process are shown in Fig. 14. For pure RTILs of $BPyBF_4$, a colorless solution was observed, and a brown solution was observed after adding Pd^{2+} and Ni^{2+}, indicating that the starting materials can be dissolved in the RTILs. Interestingly, after the thermal decomposition process, a light brown color was observed, demonstrating that some metal ions in $BPyBF_4$ have been consumed in the thermal decomposition process, which may be due to the reaction between the metal ions and $BPyBF_4$ or MWCNTs.

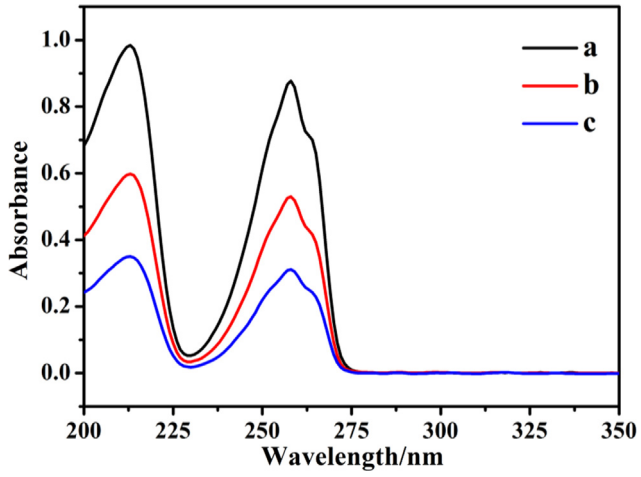

Fig. 15 – UV–vis absorption spectra of (a) pure $BPyBF_4$, (b) $BPyBF_4$ containing Pd^{2+} and Ni^{2+} before thermal decomposition process and (c) $BPyBF_4$ containing Pd^{2+} and Ni^{2+} after thermal decomposition process.

Ultraviolet–visible (UV–vis) absorption spectra for the $BPyBF_4$ before and after the thermal decomposition process are presented in Fig. 15. As shown by curve **a**, for the pure $BPyBF_4$, two absorption peaks located at around 213 and 258 nm were observed. It was reported that the spectra in the far-UV region (200–250 nm) corresponded to the peptide $n \rightarrow \pi^*$ electronic transition [45]. For the $BPyBF_4$ containing Pd^{2+} and Ni^{2+} before thermal decomposition process, as shown by curve **b**, the intensities of all the absorption peaks were significantly attenuated relative to that of pure $BPyBF_4$, suggesting that the $n \rightarrow \pi^*$ electronic transition was greatly inhibited by the introduced ions of Pd^{2+} and Ni^{2+}. Generally, the empty orbits, such as *d*-orbit, in Pd^{2+} or Ni^{2+} can react with the electron pairs in the N atom of $BPyBF_4$, which may reduce the intensity of the absorption peak. This kind of interaction is very similar to that occurring in the formation process of the self-assembled monolayer between the gold substrate and calmodulin [46]. For the filtered $BPyBF_4$ after the thermal decomposition process, curve **c**, the intensities of the absorption peaks were further attenuated, suggesting that the interaction between metal ions and $BPyBF_4$ and the molecular structure of $BPyBF_4$ was demolished markedly, owing to the formation of Pd_xNi_y catalyst particles from the $BPyBF_4$ solution. The FT-IR spectra of the $BPyBF_4$ used for preparing the catalyst of Pd_3Ni_2/MWCNTs are presented in Fig. 16. Based on the previous work [47], the bands at 1176 and 1577 cm^{-1} can be assigned to the in-plane C–H deformation vibration and in-plane C–N stretching vibration of the imidazole ring, respectively [47]. The bands at 767 and 858 cm^{-1} are assigned to the BF_4^{-1} stretching vibration and C–H in-plane vibration of the pyridinium ring, respectively. And the broad band at 1469 cm^{-1} is assignable to the CH_3 bending vibrations [47]. It can be seen that for the precursor before the thermal decomposition process (curve **b**), i.e., $BPyBF_4$ containing Pd^{2+} and Ni^{2+}, the intensities of all the absorption peaks were evidently augmented compared to those of pure $BPyBF_4$ (curve **a**), indicating that some groups in $BPyBF_4$ have reacted with the introduced Pd^{2+} and Ni^{2+}. How does one understand this result? Probably, the steric structure of $BPyBF_4$ has been

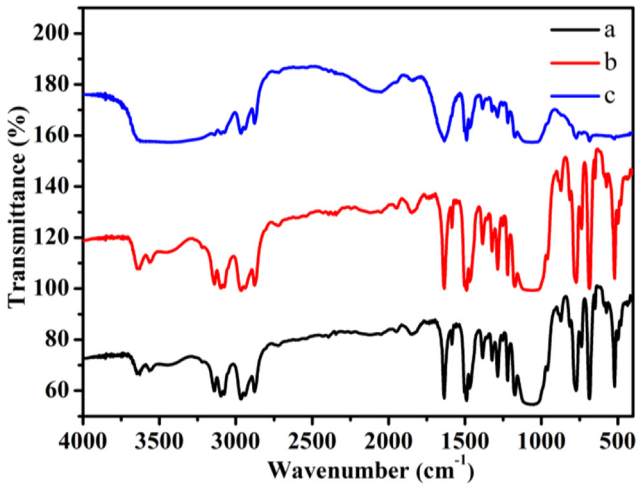

Fig. 16 – FT-IR spectra of (a) pure $BPyBF_4$, (b) $BPyBF_4$ containing Pd^{2+} and Ni^{2+} before thermal decomposition process, and (c) $BPyBF_4$ containing Pd^{2+} and Ni^{2+} after thermal decomposition process.

readjusted by the introduced ions of Pd^{2+} and Ni^{2+}, showing more detectable groups since the band intensity of FT-IR spectra is proportional to the groups of $BPyBF_4$ [48]. After the thermal decomposition process, the band intensities of the FT-IR spectra (curve **c**) were decreased instead, implying that some groups of $BPyBF_4$ have been consumed by the reaction between the introduced Pd^{2+}, Ni^{2+} or MWCNTs and $BPyBF_4$. The analysis from the FT-IR spectra strongly not only demonstrated that there is an interaction between the doped ions (Pd^{2+} and Ni^{2+}) and ionic liquid of $BPyBF_4$, but also indicated that the above mentioned interaction was destroyed by the thermal decomposition process in some degree. In other words, there were some reactions in the developed thermal decomposition process.

What is the reducing reagent in the aforementioned thermal decomposition process? Evidently, there must be some substances releasing electrons to the ions of Pd^{2+} and Ni^{2+}, leading to the formation of Pd_xNi_y. Fig. 17 displays the FT-IR spectra for the pure MWCNTs before thermal decomposition process and the resultant catalysts of Pd_3Ni_2/MWCNTs. Based on the previously published works, the strong peak at 3463 cm^{-1} can be attributed to H–O stretching vibration of absorbed water on the MWCNTs [49], and the peaks occurring in the wavenumber range of 1050–1250 cm^{-1} are assigned to the stretching vibrations of C–C [49] or the stretching vibrations of C–O in ethers and phenols [49]. An obvious peak at 2360 cm^{-1} is displayed for pure MWCNTs, interestingly, after the thermal decomposition process this band almost disappeared, illustrating that some groups of the MWCNTs were consumed by the thermal decomposition process. That is to say, carbon nanotube itself was employed as the reducing reagent in the thermal decomposition procedure.

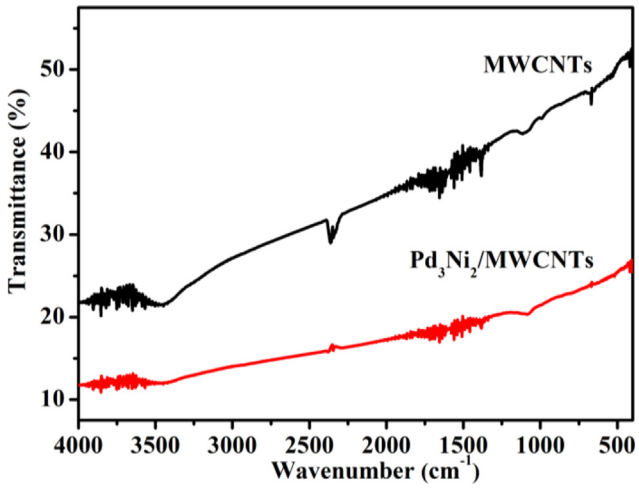

Fig. 17 – FT-IR spectra for the pure MWCNTs before thermal decomposition process (black curve) and the resultant sample of Pd_3Ni_2/MWCNTs (red curve). (For interpretation of the references to color in this figure legend, the reader is referred to the web version of this article.)

Conclusion

For the first time, using RTILs of N-butylpyridinium tetrafluoroborate ($BPyBF_4$) as solvent, Pd_xNi_y bimetallic composite nanoparticle catalysts were fabricated by a simple thermal decomposition process in the presence of MWCNTs. The results demonstrated that due to the small particle size and higher crystallinity, the Pd_3Ni_2/MWCNTs catalyst exhibited the best electrocatalysis toward formic acid oxidation in an acidic electrolyte among all the prepared Pd_xNi_y/MWCNTs catalysts. In the electrolyte of 0.5 M H_2SO_4, a larger hydrogen evolution peak with the most positive onset potential was displayed at the catalyst of Pd_3Ni_2/MWCNTs when compared to other catalysts. This may lead to a facilitated generation of OH^-, which was considered as the possible reason for the enhanced peak current of FAOR on Pd_3Ni_2/MWCNTs. Results of chronopotentiometric tests indicated that the electrode potential of Pd_3Ni_2/MWCNTs-coated electrode was lower than other samples, which may be responsible for its electrocatalytic ability toward FAOR in some degree based on the electrochemical principle. Apart from describing the electrochemical performance of the composite NPs toward FAOR, the disclosed information, including a proposed microbattery formed in the bimetallic catalysts when exposed to an electrolyte, and the application of RTILs as solvent in a thermal decomposition process to synthesize NPs, is also the main contribution of this work, which is expected to be helpful for understanding the role of the second or third metal in the Pd-based catalysts and developing novel catalysts towards small organic molecules oxidation reaction.

Acknowledgments

This work was financially supported by the National Natural Science Foundation of China (No. 21173066), Natural Science Foundation of Hebei Province of China (No. B2011205014). Z.

Guo acknowledges the support from US National Science Foundation (EAGER:CBET 11-37441) managed by Dr Rosemarie D. Wesson.

REFERENCES

[1] Hsu C, Huang C, Hao Y, Liu F. Impact of surface roughness of Au core in Au/Pd core-shell nanoparticles toward formic acid oxidation – experiment and simulation. J Power Sources 2013;243:343–9.

[2] Xia BY, Wu HB, Yan Y, Lou XW, Wang X. Ultrathin and ultralong single-crystal Pt nanowire assemblies with highly stable electrocatalytic activity. J Am Chem Soc 2013;135:9480–5.

[3] Chang J, Sun X, Feng L, Xing W, Qin X, Shao G. Effect of nitrogen-doped acetylene carbon black supported Pd nanocatalyst on formic acid electrooxidation. J Power Sources 2013;239:94–102.

[4] Tian N, Zhou Z-Y, Yu N-F, W L-Y, Sun S-G. Direct electrodeposition of tetrahexahedral Pd nanocrystals with high-index facets and high catalytic activity for ethanol electrooxidation. J Am Chem Soc 2010;132:7580–1.

[5] Pavese AG, Solis VM, Giordano MC. Oxidation of formic acid on palladium anodes in acidic medium. Effect of Pd(II) ions. Electrochim Acta 1987;32:1213–7.

[6] Wang S, Manthiram A. Graphene ribbon-supported Pd nanoparticles as highly durable, efficient electrocatalysts for formic acid oxidation. Electrochim Acta 2013;88:565–70.

[7] Hong W, Liu Y, Wang J, Wang E. Ultrasound assisted synthesis of carbon supported Pd nanoparticles toward ethanol electrooxidation. Electrochem Commun 2013;31:59.

[8] Wang X, Tang Y, Gao Y, Lu T. Carbon-supported Pd-Ir catalyst as anodic catalyst in direct formic acid fuel cell. J Power Sources 2008;175:784–8.

[9] Li L, Yuan YEJ, Luo X, Yang Y, Fan L. Electrosynthesis of Pd/Au hollow cone-like microstructures for electrocatalytic formic acid oxidation. Electrochim Acta 2011;56:6237–44.

[10] Tominaka S, Mommab T, Osaka T. Electrodeposited Pd-Co catalyst for direct methanol fuel cell electrodes: preparation and characterization. Electrochim Acta 2008;53:4679–786.

[11] Maiyalagan T, Scott K. Performance of carbon nanofiber supported Pd-Ni catalysts for electro-oxidation of ethanol in alkaline medium. J Power Sources 2010;195:5246–51.

[12] Shen L, Li H, Lu L, Luo Y, Tang Y, Chen Y, et al. Improvement and mechanism of electrocatalytic performance of Pd-Ni/C anodic catalyst in direct formic acid fuel cell. Electrochim Acta 2013;89:497–502.

[13] Xiao Y, Yu G, Yuan J, Wang J, Chen Z. Fabrication of Pd-Ni alloy nanowire arrays on HOPG surface by electrodeposition. Electrochim Acta 2006;51:4218–27.

[14] Ghilane J, Lacroix J-C. Formation of a bifunctional redox system using electrochemical reduction of platinum in ferrocene based ionic liquid and its reactivity with aryldiazonium. J Am Chem Soc 2013;135:4722–8.

[15] Prasad V, Kale RR, Mishra BB, Kumar D, Tiwari VK. Diacetoxyiodobenzene mediated one-pot synthesis of diverse carboxamides from aldehydes. Org Lett 2012;14:2936–9.

[16] Jones A, Kronenwetter H, Manchanayakage R. Electrochemical reductive coupling of 2-cyclohexen-1-one in a mixture of ionic liquid and water. Electrochem Commun 2012;25:8–10.

[17] Ding K, Yang G. Using RTILs of EMIBF4 as "water" to prepare palladium nanoparticles onto MWCNTs by pyrolysis of $PdCl_2$. Electrochim Acta 2010;55:2319–24.

[18] Chae W-S, An M-J, Lee S-W, Son M-S, Yoo K-H, Kim Y-R. Templated carbon nanofiber with mesoporosity and semiconductivity. J Phys Chem B 2006;110:6447–50.

[19] Xue M, Chen G, Yang H, Zhu Y, Wang D, He J, et al. Superconductivity in potassium-doped few-layer graphene. J Am Chem Soc 2012;134:6536–9.

[20] Park JH, Thorgaard SN, Zhang B, Bard AJ. Single particle detection by area amplification: single wall carbon nanotube attachment to a nanoelectrode. J Am Chem Soc 2013;135:5258–61.

[21] Wang S, Yu D, Dai L. Polyelectrolyte functionalized carbon nanotubes as efficient metal-free electrocatalysts for oxygen reduction. J Am Chem Soc 2011;133:5182–5.

[22] Liang Y, Li Y, Wang H, Dai H. Strongly coupled inorganic/nanocarbon hybrid materials for advanced electrocatalysis. J Am Chem Soc 2013;135:2013–36.

[23] Ding K, Cao M. Pyrolysis of chloroplatinic acid to directly immobilize platinum nanoparticles onto multi-walled carbon nanotubes. Russ J Electrochem 2008;44:977–80.

[24] Li R, Wei Z, Huang T, Yu A. Ultrasonic-assisted synthesis of Pd-Ni alloy catalysts supported on multi-walled carbon nanotubes for formic acid electrooxidation. Electrochim Acta 2011;56:6860–5.

[25] Wang Y, Yang F, Yang H, Zheng C, Cao Y, Ding K. Oxygen reduction reaction (ORR) on huge gold (Au) particles prepared by a pyrolysis process of $AuCl_3$ dissolved in distilled water in the presence of MWCNTs. J Chin Chem Soc 2013;60:73–80.

[26] Zhang Z, Xin L, Sun K, Li W. Pd-Ni electrocatalysts for efficient ethanol oxidation reaction in alkaline electrolyte. Int J Hydrogen Energy 2011;36:12686–97.

[27] Tang K, Sun J, Yu X, Li H, Huang X. Electrochemical performance of $LiFePO_4$ thin films with different morphology and crystallinity. Electrochim Acta 2009;54:6565.

[28] Shi R, Huang G, Lin J, Zhu Y. Photocatalytic activity enhancement for Bi_2WO_6 by fluorine substitution. J Phys Chem C 2009;113:19633–8.

[29] Radmilovic V, Gasteiger HA, Ross PN. Structure and chemical composition of a supported Pt-Ru electrocatalyst for methanol oxidation. J Catal 1995;154:98–106.

[30] Zhang D, Okajima T, Matsumoto F, Ohsaka T. Electroreduction of dioxygen in 1-*n*-alkyl-3-methylimidazolium tetrafluoroborate room-temperature ionic liquids. J Electrochem Soc 2004;151:D31–7.

[31] Shipway AN, Lahav M, Gabai R, Willner I. Investigations into the electrostatically induced aggregation of Au nanoparticles. Langmuir 2000;16:8789–95.

[32] Wang M, Li Y-J, Xie Z-X, Liu C, Yeung ES. Fabrication of large-scale one-dimensional Au nanochain and nanowire networks by interfacial self-assembly. Mater Chem Phys 2010;119:153–7.

[33] Li Y-J, Huang W-J, Sun S-G. A universal approach for the self-assembly of hydrophilic nanoparticles into ordered monolayer films at a toluene/water interface. Angew Chem Int Ed 2006;45:2537–9.

[34] Wang R, Wang H, Wang X, Liao S, Linkov V, Ji S. Effect of the structure of Ni nanoparticles on the electrocatalytic activity of Ni@Pd/C for formic acid oxidation. Int J Hydrogen Energy 2013;38:13125–31.

[35] Ding K, Yang G, Wei S, Mavinakuli P, Guo Z. Cyclic voltammetric preparation of palladium nanoparticles for ethanol oxidation reaction. Ind Eng Chem Res 2010;49:11415–20.

[36] Hu C, Yuan S, Hu S. Studies on electrochemical properties of MWNTs-Nafion composite films based on the redox behavior of incorporated Eu3+ by voltammetry and electrochemical impedance spectroscopy. Electrochim Acta 2006;51:3013–21.

[37] Adekunle AS, Ozoemena KI. Electron transfer behaviour of single-walled carbon nanotubes electro-decorated with

nickel and nickel oxide layers. Electrochim Acta 2008;53:5774–82.
[38] Gabrielli C, Grand PP, Lasia A, Perrot H. Investigation of hydrogen adsorption and absorption in palladium thin films: II. Cyclic voltammetry. J Electrochem Soc 2004;151:A1937–42.
[39] Krebs E, Silvi B, Raybaud P. Mixed sites and promoter segregation: a DFT study of the manifestation of Le Chatelier's principle for the Co(Ni)MoS active phase in reaction conditions. Catal Today 2008;130:160–9.
[40] Ju P, Zuo Yu, Tang Y, Zhao X. The enhanced passivation of 316L stainless steel in a simulated fuel cell environment by surface plating with palladium. Corros Sci 2013;66:330–6.
[41] Shen SY, Zhao TS, Xu JB. Carbon-supported bimetallic PdIr catalysts for ethanol oxidation in alkaline media. Electrochim Acta 2010;55:9179–84.
[42] Bard AJ, Faulkner LR. Electrochemical methods fundamentals and applications. 2nd ed.: John Wiley & Sons, Inc.
[43] Xua C, Liu Y, Wang J, Geng H, Qiu H. Nanoporous PdCu alloy for formic acid electro-oxidation. J Power Sources 2012;199:124–31.
[44] Qin Y-H, Jiang Y, Niu D-F, Zhang X-S, Zhou X-G, Niu L, et al. Carbon nanofiber supported bimetallic PdAu nanoparticles for formic acid electrooxidation. J Power Sources 2012;215:130–4.
[45] Wu X, Du P, Wu P, Cai C. Effects of 1-butyl-3-methylimidazolium tetrafluoroborate on the oxidation of glucose catalyzed by glucose oxidase. Electrochim Acta 2008;54:738–43.
[46] Ding K, Jia Z, Wang Q, He X, Tian N, Tong R, et al. Electrochemical behavior of the self-assembled membrane formed by calmodulin (CaM) on a Au substrate. J Electroanal Chem 2001;513:67–71.
[47] Shi F, Deng Y. Abnormal FT-IR and FTRaman spectra of ionic liquids confined in nano-porous silica gel. Spectrochim Acta Part A 2005;62:239–44.
[48] Nanbu N, Sasaki Y, Kitamura F. In situ FT-IR spectroscopic observation of a room-temperature molten salt/gold electrode interphase. Electrochem Commun 2003;5:383–7.
[49] Biniak S, Świątkowski A, Pakuła M, Sankowska M, Kuśmierek K, Trykowski G. Cyclic voltammetric and FTIR studies of powdered carbon electrodes in the electrosorption of 4-chlorophenols from aqueous electrolytes. Carbon 2013;51:301–12.